Current Research in Food Science 9 (2024) 100801

Contents lists available at ScienceDirect

Current Research in Food Science

journal homepage: www.sciencedirect.com/journal/current-research-in-food-science

Mapping deterioration in electrospun zein nonwoven nanostructures encapsulating corn oil

Louis A. Colaruotolo [a], Singam Suranjoy Singh [a], Stacie Dobson [a], Loong-Tak Lim [a], Iris J. Joye [a], Michael A. Rogers [a], Maria G. Corradini [a,b,*]

[a] Department of Food Science, University of Guelph, Guelph, ON, Canada
[b] Arrell Food Institute, University of Guelph, Guelph, ON, Canada

ARTICLE INFO

Keywords:
Nonwovens
Shelf-life
Microspectroscopy
Lipid oxidation
Mechanical properties
Structure

ABSTRACT

Electrospun nonwovens of biopolymers are gaining popularity in filtration, coatings, encapsulation, and packaging materials. However, their applications are hindered by limited stability, particularly when loaded with lipids. This research aimed to apply a multiscale approach to gain insights into deteriorative processes, e.g., oxidation, limiting the shelf life of these complex materials, using corn oil-loaded electrospun zein nonwovens as a model system. Oil-doped zein electrospun nonwovens were stored in the dark at 23 °C and 33% relative humidity for 28 days and tested at selected intervals to monitor their morphology and mechanical properties. Lipid oxidation was assessed using the thiobarbituric acid reactive species (TBARS) assay. The photophysical properties of intrinsic, i.e., tyrosine (Tyr), and extrinsic, i.e., boron-dipyrromethene undecanoic acid 581/591 (BODIPY C11), lumiphores were also monitored to evaluate changes in local molecular rigidity, and oxidation, respectively. The protein secondary structure was determined with Fourier transform infrared spectroscopy (FTIR). Scanning electron microscopy (SEM) analysis of the oil-loaded electrospun nonwovens revealed that the diameter of the ribbon-like fiber significantly decreased during storage from 701 ± 23 nm to 620 ± 44 nm. Breakage of the electrospun fibers was observed and correlated with increased brittleness and molecular rigidity of the nonwoven material, reflected by an increase in Tyr emission intensity and phosphorescence lifetime. Changes in tensile strength, brittleness and matrix rigidity also correlated with a zein secondary structure transition from unordered to ordered β-sheets. Raman and luminescence micrographs showed oil migration during storage, thereby increasing lipid oxidation. The correlation between local rigidity and lipid distribution/oxidation suggests that reorganizing protein structures increased material brittleness and displaced encapsulated oils within the electrospun fiber. Understanding deteriorative mechanisms aids in developing innovative strategies to improve the stability of these novel food-grade materials.

1. Introduction

Advances in fabrication technology allow the production of model foods with designed structural elements to, for example, tailor sensory properties and extend shelf-life. Among them, electrospinning of food-grade materials (e.g., edible proteins and carbohydrates) is gaining traction, leading to the manufacture of various structures from fibers, ribbons, and beads to their mixture and diameters between 100 and 1500 nm (Aceituno-Medina et al., 2013; Tang et al., 2019). During electrospinning, a high electrostatic force draws the polymer solutions from a charged wire or spinneret, stretching the solution into ultrafine structures (Li et al., 2009). Electrospun nonwovens contain fibers with submicron diameters that entangle during fabrication to produce a nonwoven sheet. These materials are gaining popularity in filtration, coatings, encapsulation, and packaging applications (Lim et al., 2019).

Nonwovens of food-grade biopolymers allow the inclusion of bioactive compounds within the fibers to ensure compatibility and improve their functional properties (e.g., nutraceutical, antimicrobial, or antioxidant activities). For example, gelatin nanofibers with encapsulated essential oils have been produced as edible packaging with antimicrobial properties, while a whey protein isolate-pullulan blend was explored for the encapsulation of resveratrol in product fortification (Seethu et al., 2020; Tang et al., 2019). Despite promising applications, the stability of nonwovens is limited due to deteriorative phenomena

* Corresponding author. Department of Food Science, University of Guelph, Guelph, ON, Canada.
E-mail address: mcorradi@uoguelph.ca (M.G. Corradini).

https://doi.org/10.1016/j.crfs.2024.100801
Received 10 May 2024; Received in revised form 14 June 2024; Accepted 27 June 2024
Available online 28 June 2024

affecting both the biopolymer carrier and the encapsulated lipids (Moomand and Lim, 2014; Xu et al., 2008). For example, García Moreno et al. (2016) reported the limited oxidative stability of electrospun fibers containing fish oil and its effects on their physical stability. Similarly, Drosou et al. (2022) observed that the structural integrity of the electrospun encapsulant diminished during storage.

Additives, such as plasticizers and antioxidants, are useful for stabilizing nonwoven structures. However, growing consumer concerns regarding food sustainability and clean food labels require alternative methods besides the incorporation of additives to increase stability (Cavaliere and Ventura, 2018; Grant et al., 2021). Thus, understanding the limiting factors influencing the stability of food-grade materials and their products must remain a priority, as the list of acceptable additives that extend shelf life is continually decreasing. Identifying the underlying mechanisms of deterioration is crucial in informing handling best practices, storage conditions, packaging material selection, and other mitigation strategies.

Since composite nonwovens contain multiple phases (e.g., encapsulant and encapsulate), concurrent deteriorative phenomena may occur. Thus, a multiscale approach that considers phenomena at the macro-, micro-, nano- and molecular levels will facilitate an improved understanding of deterioration in these matrices. Moreover, monitoring deterioration at multiple length scales provides distinct perspectives on how physical and chemical changes evolve in a matrix on their own and concerning each other. For example, previous work using a multiscale approach to understand ageing in biodegradable gelatin films concluded that protein stiffening is responsible for adverse changes in tensile stress and brittleness during storage (Colaruotolo, 2019; Colaruotolo et al., 2021). For nonwoven composites, the deteriorative mechanisms will differ based on specific constituting biopolymers and encapsulates and must be assessed without altering existing structures. To this end, optical spectroscopic tools are versatile due to their non-destructive and minimally invasive testing procedures, allowing sample analysis *in situ* with minimal sample preparation. These techniques provide complementary assessments of the nonwoven state and its existing structure.

Zein was chosen as the biopolymer in this study due to its popularity as an encapsulant of lipid-soluble bioactive compounds, while corn oil was the encapsulate. Corn oil was selected due to its common use as a hydrophobic bioactive carrier (Liu et al., 2019; Moomand and Lim, 2015; Wang et al., 2019); however, no bioactives were added to facilitate data interpretation. In zein fibers with encapsulated oil, solvent (alcohol) evaporation from the polymer-oil solution during spinning decreases the solvent quality near the jet surface, causing the oil to migrate to the center of the structure during formation (Moomand and Lim, 2014), effectively encapsulating it. This study aimed to quantify and better understand the relationships between deteriorative processes in zein nonwovens with encapsulated corn oil and inform best practices to extend shelf life and mitigate deleterious effects, such as oxidation, matrix stiffness or increased brittleness.

2. Materials and methods

2.1. Materials

Zein (90% purity) and corn oil (99% purity) were obtained from Millipore Sigma (Etobicoke, ON, Canada) and used without further purification or modification. Magnesium chloride, trichloroacetic acid, hydrochloric acid (99.9% purity), BODIPY 581/591 undecanoic acid (BODIPY C11), LipidTOX™ Deep Red were acquired from Thermo Fisher Scientific (Ottawa, ON, Canada), while 2-thiobarbituric acid (98% purity) was obtained from M.P. Biomedicals (Solon, OH, USA). Nitrogen (99.998% purity) was supplied by Praxair (Danbury, CT, USA). Anhydrous 2-propanol (HPLC grade) from Millipore Sigma and double-distilled water were used as solvents.

2.2. Zein nonwoven fabrication and storage

Spin dope solutions, i.e., homogeneous and stable solutions to be spun, were prepared as detailed in Moomand and Lim (2015) with modifications. Zein at 20% (w/w) was dissolved in 80% (w/w) 7:3 2-propanol:water solution by stirring at 1200 rpm for 15 min. Corn oil was added during mixing in the dark at 1200 rpm at room temperature (21 ± 2 °C) for 15 min to achieve an oil:protein ratio of 3:10 (w/w). Electrospinning was conducted using an N.S. lab Nanospider (Elmarco s. r.o, Liberec, Czech Republic) at 21 ± 2 °C and 35 ± 5% relative humidity (RH). The polymer solution was electrospun through a wire and carriage spinneret (0.7 mm diameter orifice) at 150 mm/s. This setup, i.e., the wire and carriage spinneret, was selected since it allows for higher throughputs than needle configurations, better mimicking industrial procedures and conditions. Additionally, this setup avoids clogging and reduces the probability of developing complex fiber structures that would unnecessarily complicate analysis and monitoring deterioration effects (Prahasti et al., 2020; Menaka and Srinivasan, 2023). The spinning voltage was set at 50 kV to attain the higher levels required by a wire carriage configuration. The nonwoven samples were stored in the dark to reduce photodegradation, within sealed containers holding a saturated solution of magnesium chloride that allowed maintaining a 33% RH within the chamber. The samples were placed on a mesh affixed 3 m above the bottom of the container that separated them from the solution and stored at 23 ± 2 °C.

2.3. Mechanical characterization of zein nonwovens

The mechanical properties of the electrospun nonwovens during storage were assessed using a Modular Compact Rheometer (MRC 302, Anton Paar, Graz, Austria). Strips (20 × 50 mm) of electrospun material were affixed between the testing platform and a 20 mm plate (PP20/S), separated by a 10 mm gap. The samples deformed in tensile mode at a constant velocity of 12 mm/min until mechanical failure. Triplicate samples were tested after 0, 7, 14, 21, and 28 days of storage with a sample size of n = 5. Acquisition time (s), extension (mm), and force (mN) were recorded and used to calculate the engineering stress (σ_E):

$$\sigma_E = \frac{F}{A_0} \tag{1}$$

where F is the normal force in mN, A_0 corresponds to the original cross-sectional area of the nonwoven sheet in m^2, and the Hencky strain (ε_H) as:

$$\varepsilon_H = ln\left(\frac{L}{L_0}\right) \tag{2}$$

where L is the length of material in mm at time t (s), and L_0 is its initial length (mm).

Young's modulus (Y) assessed the material extensibility (Steffe, 1996) and was calculated as:

$$Y = \frac{\sigma_{Ef} - \sigma_{Ei}}{\varepsilon_{Hf} - \varepsilon_{Hi}} \tag{3}$$

where the subscripts i and f correspond to the initial and final measures, respectively.

The jaggedness of the force vs. deformation curve described the brittleness of the materials (Calzada and Peleg, 1978). The percent of direction reversals in this relationship, which corresponds to the percentage of the data points identified as local extrema, was calculated by counting the events where the force decreased from its previous value, after which it increased again in the subsequent point, as described in Corradini and Peleg (2006).

2.4. Morphology of zein nonwovens

Scanning electron microscopy (Model S-570) (Hitachi High Technologies Corp., Tokyo, Japan) with an accelerating voltage of 20 kV and a 30,000× magnification evaluated the electrospun nonwoven morphology after the samples were prepared with a 20 nm gold deposit layer using a vacuum-assisted sputter coater (Model K550, Emitech, Ashford, Kent, England). Image analysis was done using Pro-Plus 5.1 (Media Cybernetics Inc., Rockville, MD, USA) and ImageJ (U.S. National Institutes of Health, Bethesda, MD, USA).

2.5. Thiobarbituric acid reactive species (TBARS) assay

This assay followed Hadad and Goli's (2019) protocol with modifications. Electrospun material (5 mg) was dissolved in 4 mL of trichloroacetic acid (15% w/v) and 0.375% (w/v) thiobarbituric acid (TBA) in 0.25 M HCl in a glass test tube. Samples were placed in a water bath at 100 °C for 30 min and then submerged in cold water until they reached room temperature. The absorbance spectra of the samples were recorded from 300 to 800 nm at 21 °C with a 5 nm slit using a Duetta-Fluorescence and Absorbance Spectrometer (Horiba Scientific Inc., Edison, NJ, USA). The absorbance spectrum of the TBA reagent was recorded as a control and subtracted from the sample spectra before normalization to the initial absorbance (day 0) at 300 nm. The absorbance intensity at 530 nm was reported in triplicate samples (n = 6) tested at 0, 7, 14, 21, and 28 days of storage.

2.6. Characterization of deterioration using luminescence spectroscopy techniques

2.6.1. Steady-state measurements

Luminescence spectroscopy provides information on the molecular mobility and lipid oxidation of the matrix by recording the fluorescence emission spectra of intrinsic and extrinsic probes. Tyrosine (Tyr) is zein's predominant aromatic amino acid and an intrinsic reporter of molecular mobility. BODIPY 581/591 undecanoic acid (BODIPY C11) has dual emission bands at 515 and 595 nm, corresponding to oxidized and unaltered compounds, respectively. This oxidation-sensitive probe, dispersed in corn oil at 16.66 μM and mixed into the zein in 2-propanol dispersion, was electrospun directly onto strips (1 cm × 2 cm) of black paper (Astrobrights #22321, Neenah Inc, Alpharetta, GA, USA), using the settings described above. The strips were mounted on quartz slides (13.5 mm × 30 mm × 0.5 mm) (FireflySci, Staten Island, NY, USA) and placed at a 45° angle in 1 cm light path quartz cuvettes (FireflySci) before equilibrating them to 21 °C. The fluorescence emission spectra of the probes were recorded using a Fluoromax-4 spectrophotometer (Horiba Scientific Inc., Edison, NJ, USA) using long-pass filters (Thorlabs, Newton, NJ, USA) to decrease recording light scattering and the different excitation and emission wavelengths and slits for each probe, as summarized in Table 1. The emission spectra without added probes (i.e., controls) were collected using the same experimental conditions, and subtracted from those of the samples to eliminate the background signal of the matrix. Triplicates (sample size of n = 6) were tested at 0, 2, 5, 7, 10, 14, 17, 21, 25, and 28 days of storage.

2.6.2. Time-resolved measurements

Tyr phosphorescence lifetimes were measured using a Cary Eclipse spectrophotometer (Agilent, Santa Clara, CA, USA) for the nonwovens attached to a 13.5 mm × 30 mm × 0.5 mm quartz slide (FireflySci) and placed at a 45° angle in 1 cm-light path cuvettes. Samples were equilibrated at 5 °C using a Peltier system (Quantum Northwest, Liberty Lake, WA, USA) under a constant stream of nitrogen to displace the oxygen. Table 1 includes the experimental conditions for recording Tyr phosphorescence. The phosphorescence lifetime decays were characterized using a multi-exponential function (3 components) using OriginPro 2021 (OriginLab Corp., Northampton, MA, USA), and the average lifetime reported.

Table 1
Luminescent probes and testing conditions used for each analytical method.

Method	Probe	Testing conditions			
		λ_{exc} (nm)	λ_{em} range (nm)	Exc. And Em. Slit (nm)	Long pass cut-off (nm)
Steady-state fluorescence spectroscopy	Tyr	270	290–500	1:2	290
	BODIPY C11[a]	490	500–650	1:2	495
		575	585–650	1:2	590
Time-resolved phosphorescence spectroscopy	Tyr	270	470	10:20	Not used
Fluorescence microscopy	BODIPY C11[a]	488	495–530	n/a	495
		543	580–620	n/a	590
	LipidTOX™ deep red	633	645–700	n/a	Not used

[a] First and second λ_{exc} correspond to the non-oxidized and oxidized forms, respectively.

2.6.3. Fluorescence microscopy

Luminescent probes with an affinity for lipids (i.e., LipidTOX™ deep red and BODIPY C11) were loaded into the nonwovens. The neutral lipid stain LipidTOX™ deep red (10 μL) was added to 0.3 g of corn oil before including the oil in the spin dope solution. The LipidTOX™ allows visualization of the location and migration of oil in the nonwoven fibers throughout storage. BODIPY C11 in corn oil at 100 μM monitored and mapped lipid oxidation within the matrices. Table 1 summarizes the excitation and emission wavelengths for both probes. Micrographs of the nonwovens were obtained using a DM IRE2 luminescence microscope (Leica Microsystems, Wetlzar, Germany) by overlying the signals at each excitation wavelength.

2.7. Confocal Raman Microspectroscopy (CRM)

Raman mapping of samples on a WITec alpha300 R microscope (Witech, Ulm, Germany) equipped with an ultra-sensitive EMCCD detector and 532 nm solid-state diode laser excitation source collected the Raman scattered light in the backscattering geometry using a 600 groove/mm grating after focusing on an area consisting of ribbon structures with a 100× magnification lens. A Raman scatter map of the selected area was obtained from 100 scans per line and 100 lines per image using 20 mW laser power and 0.05 s integration time. The Raman image was generated using the filter manager and true component analysis function of the WITec software using different colors and gradients to differentiate peaks and intensities. Based on the sample characteristics and purpose of the measurement, the amide I region (~1610 - 1690 cm^{-1}) for protein and the C–H stretching region (~2830-3090 cm^{-1}) for lipids were monitored, as well as the disulfide region (490-550 cm^{-1}) and Tyr ring vibration/doublet band (I_{850}/I_{830}).

2.8. Fourier transform infrared (FTIR) spectroscopy

The secondary structure of the protein in the nonwovens was analyzed using an FTIR spectrophotometer (Prestige21, Shimadzu Corporation, Kyoto, Japan) equipped with an attenuated total reflectance (ATR) attachment (MIRacle, Pike, Madison, WI). Reflectance spectra of the nonwoven matrices were collected at frequencies from 800 to 4000 cm^{-1}. The Happ-Genzel apodization function was applied at a 4 cm^{-1} resolution and 6 mm aperture, averaging 32 scans. Spectra collected using Lab Solutions software (Shimadzu Corporation, Kyoto, Japan) were processed and analyzed using OriginPro 2021 (OriginLab Corp.). Vibrations of the C=O and C–N bonds in the 1600-1700 cm^{-1} range, i.e., amide I region, monitored the predominant protein secondary structure

during storage. Fourier self-deconvolution was used to identify the hidden peaks in the amide I region using a smoothing window of 5 and a smoothing factor of 0.15. The peaks fitted with Voigt functions allowed determining each peak contribution to the overall signal of the amide I region.

2.9. Modeling degradation kinetics

The kinetics of the main quality attributes studied, $Y(t)$, specifically, matrix rigidity (expressed as an increment in the intensity of the intrinsic fluorophores), lipid oxidation, and formation of disulfide bonds were described using a logistic model (Aragao et al., 2008):

$$Y(t) = 1 + \frac{Y_{max} - 1}{(1 + e^{k(t_c - t)}) - (1 + e^{k*t_c})} \quad (4)$$

where Y_{max} corresponds to the maximum value of the attribute of interest, k is the reaction rate, and t_c is a critical time when change becomes prevalent. The experimental data was adjusted to Eq. (4), using the nonlinear regression routine in Mathematica 13.2 (Wolfram Research, Inc. Champaign, IL, USA).

2.10. Statistical analysis

Statistically significant differences in all reported data were evaluated using one-way ANOVA and Tukey tests at $\alpha = 0.05$ for mean comparisons in OriginPro (2021) (OriginLab Corp.). The goodness of fit of the mathematical characterization of the kinetic reactions was evaluated based on the adjusted R^2 and the mean squared error.

3. Results and discussion

3.1. Morphology and mechanical properties of nonwovens

Scanning electron micrographs of fresh nonwovens showed ribbons with a width of 701 ± 23 nm, which decreased to 649 ± 58 nm and 620 ± 44 nm after 14 and 28 days, respectively (Fig. 1). The decrease in fiber width was attributed to the evaporation of the solvents (i.e., water and alcohol) initially bound or entrapped in the zein matrix and polymer rearrangements during storage. SEM is extensively used to visualize and assess the morphology of electrospun matrices to identify characteristic lengths and numbers of fibers, ribbons, beads, or their combination, after production (Pedram Rad et al., 2018). However, SEM has seldom been used to assess the deterioration of electrospun matrices during long-term storage. Besides the decrease in fiber width, physical breakage of the fibers was apparent through storage and previously reported (Bajsic et al. (2016)) for repeatedly UV-exposed polycaprolactone nonwovens with encapsulated titanium dioxide, causing extensive production of hydroperoxides and resulting in polymer chain scission and breakage. Herein, reactive oxygen species (ROS) form during the oxidation of the encapsulated oil, which alters the zein network integrity, increasing its brittleness. Therefore, ROS led to protein oxidation and solvent loss, reducing the amount of plasticizer, which could have contributed to shorter and thinner ribbons. The loss of plasticizer can also drive an increase in polymer-polymer interactions, which concurs with extensive reports that oxidation is a significant factor in protein network brittleness and increased breakage propensity (Plackett, 2011; Shah et al., 2023; Ullsten et al., 2016).

The Young's modulus of the nonwovens was estimated from their tensile stress vs. deformation curves using eq. (3). The Young's modulus of the nonwovens as a function of storage time is summarized in Table 2. After 28 days of storage, the Young's moduli of the nonwovens increased significantly by about 26%, similar to previous reports on biopolymer-based nonwovens, which exhibited a reduction in extensibility (i.e., higher rigidity) with increasing storage time (Taherimehr et al., 2021). Increased rigidity was at least partially attributed to the physical ageing of the biomaterial, a process where polymer chains rearrange within the matrix to achieve a minimum thermodynamic state, and the annealing rate depends on storage conditions, e.g., RH and temperature (Struik, 1977). Polymer chain rearrangement during physical ageing decreases the free volume between and within polymer chains, which modulates its mechanical properties, i.e., increasing material rigidity (Merrick et al., 2020). A reduction in material extensibility is reflected in the jaggedness of the tensile stress vs. deformation curves, which measure the brittleness of the material (Corradini and Peleg, 2006). The direction reversals increased from 31 ± 4 to 4.0 ± 3 % (Table 2), indicating higher brittleness, possibly due to a loss in nonwoven plasticization by the residual solvents as they evaporated during storage. This mechanical parameter provides valuable information on the increased propensity of the material to exhibit minor fractures as a function of time (Laurindo and Peleg, 2008). The increased brittleness aligns with the observed ribbon breakage in scanning electron micrographs upon storage of the nonwoven material.

3.2. Lipid oxidation within nonwovens

Lipid oxidation progressively increased by 78%, as assessed using TBARS, with the highest rate occurring in the first two weeks (Table 3). These results are comparable to those of Hadad and Goli (2019) and Aytac et al. (2017) for electrospun mucilage and poly-lactic acid (PLA) nanofibers carrying flaxseed oil and thyme essential oil, respectively. The minor discrepancies observed herein may be attributed to the incorporation of different biopolymers, lipids, and antioxidants (Aytac

Table 2
Mechanical properties of zein nonwovens with encapsulated corn oil during storage.

Storage Time (days)	Mechanical Properties	
	Young's modulus (kPa)	Brittleness (Direction Reversals) (%)
0	57 ± 13^{A}	31 ± 4^{A}
7	61 ± 12^{AB}	33 ± 4^{AB}
14	67 ± 12^{ABC}	36 ± 4^{BC}
21	72 ± 10^{BC}	39 ± 5^{CD}
28	75 ± 11^{C}	40 ± 3^{D}

*Different letters per column denote significant differences ($p < 0.05$).

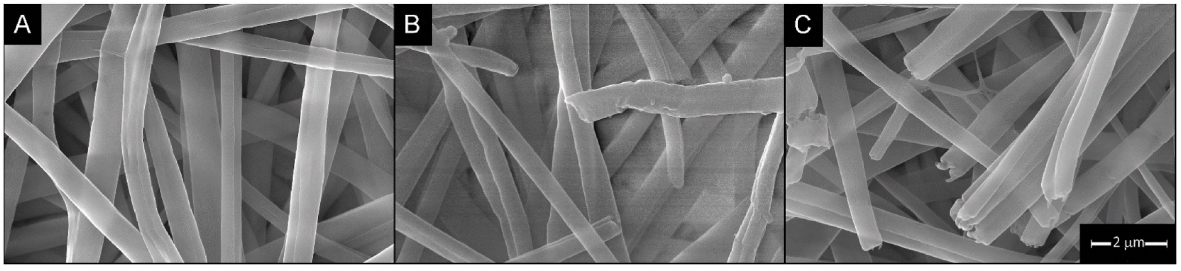

Fig. 1. Scanning electron micrographs of electrospun zein with encapsulated corn oil after A) 0, B) 14, and C) 28 days of storage.

Table 3
Lipid oxidation, assessed using TBARS, of zein nonwovens with encapsulated corn oil during storage.

Storage Time (days)	TBARS Assay
	Normalized absorbance at 533 nm (−)
0	1.00 ± 0.02^{A}
7	1.41 ± 0.01^{B}
14	1.65 ± 0.02^{C}
21	1.77 ± 0.01^{C}
28	1.78 ± 0.01^{C}

*Different letters denote significant differences ($p < 0.05$).

et al., 2017; Hadad and Goli, 2019). The effect of fiber fabrication, e.g., exposure to a 50 kV voltage, on lipid oxidation was evaluated by comparing the TBARS of the oil before and after electrospinning, revealing no significant differences. Considering the TBARS assay results, it is clear that lipid oxidation is an important deteriorative effect in nonwovens during storage. The TBARS method, however, has low selectivity, e.g., besides detecting products from lipid oxidation, TBARS also reacts with protein oxidation products. Additionally, corn oil contains both mono- and polyunsaturated fatty acids and malonaldehyde, the primary compound measured by TBARS, is only formed during the oxidation of polyunsaturated lipids and not monounsaturated fatty acids (Barrera-Arellano et al., 2019). Thus, this technique does not fully characterize lipid oxidation in multi-component materials (Fantini and Yoshioka, 1992). Incorporating liposoluble fluorophores LipidTOX™ deep red and BODIPY C11 in the nonwovens allows lipids and the oxidation state to be visualized within a system, respectively. Micrographs of the nonwovens obtained immediately after production showed a relatively even distribution of oil throughout the core of the fiber (Fig. 2A i). The displacement and uneven distribution of the oil during storage are likely associated with solvent loss and increased protein-protein interactions, which appeared to displace the oil out of the core of the zein fiber encapsulant. The red emission of the BODIPY C11 (Fig. 2A ii) corresponds to the unoxidized probe and is evidence that the oil was not initially oxidized, as confirmed by a faint green emission of the oxidized BODIPY C11 (Fig. 2A iii). After 28 days of storage, the lipid was no longer evenly distributed (Fig. 2B i), with a concomitant increase in the ratio of the emission intensities of the oxidized to unoxidized BODIPY C11 (Fig. 2B ii and iii). Oxidation within the observed area using the emission intensities of the unoxidized and oxidized BODIPY C11 could be quantified. However, since the local oil concentration did not remain constant during storage, changes in emission could be confounded by changes in probe concentration. In comparison, steady-state luminescence spectroscopy provided a more reliable quantitative measure of oxidation. The fluorescence emission intensity at 595 nm, representing the unoxidized BODIPY C11, decreased slightly during the first five days of storage, consistent with a lag or delay period in the kinetics of lipid oxidation corresponding to the initiation stage. After the lag phase, the unoxidized BODIPY C11 emission progressively decreased to 44% of its initial value (Fig. 3). Unlike the TBARS assay, BODIPY C11 does not report on secondary oxidative products, thereby reducing the risk of overestimating the extent of lipid oxidation (Domínguez-Rebolledo et al., 2010). The primary advantage of BODIPY C11 in assessing lipid oxidation is that it accounts for the depletion and formation of two forms of a single compound (BODIPY

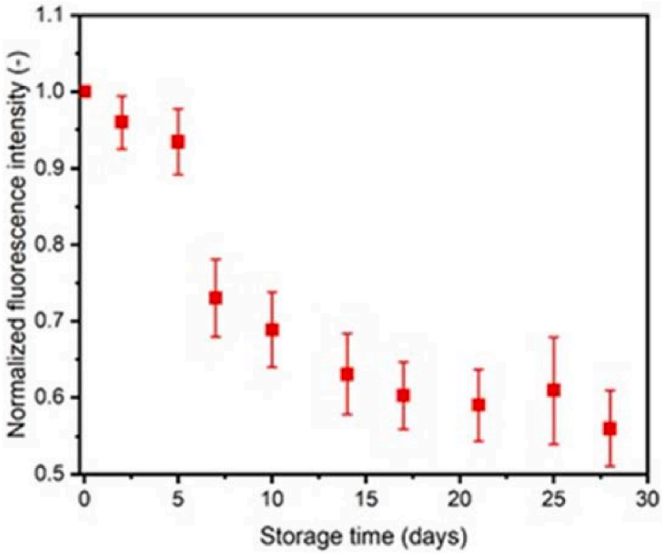

Fig. 3. Normalized fluorescence emission intensity of unoxidized BODIPY C11 (λ_{exc} = 490 nm) in electrospun zein nonwovens as a function of storage time.

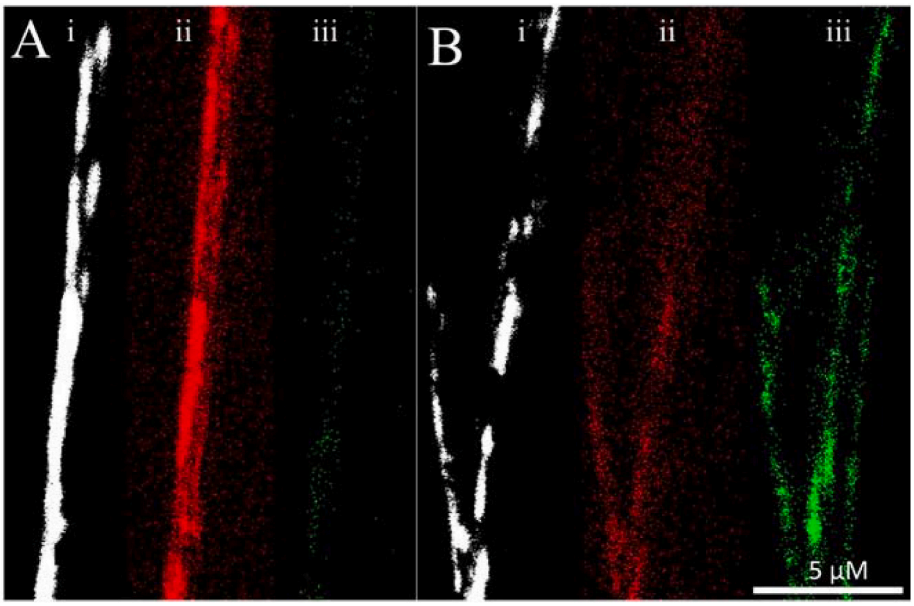

Fig. 2. Fluorescence micrographs of electrospun zein with encapsulated corn oil after A) 0 and B) 28 days of storage. i) LipidTOX™ to identify lipid location, ii) Unoxidized BODIPY C11 and iii) Oxidized BODIPY C11.

C11), whose concentration remains constant throughout the entire storage time and does not rely on measuring diverse oxidized products (e.g., hydroperoxides) with ephemeral lifetimes.

3.3. Zein structure in the nonwovens

The luminescence emission of the aromatic amino acids (AAA), i.e., phenylalanine (Phe), Tyr, and tryptophan (Trp), in a protein, is sensitive to changes in the microenvironment where the AAAs are embedded. In the case of zein, the lack of Trp in its composition requires focusing on Tyr emission intensity and lifetimes, using steady-state and time-resolved measurements, respectively. Tyr is a useful probe to characterize the molecular mobility of protein confined in a matrix (e.g., Tyr buried in the hydrophobic core of the protein increases fluorescence emission, and phosphorescence lifetime) (Corradini et al., 2017; Draganski et al., 2015). In the present study, Tyr fluorescence emission from the nonwovens, monitored during storage, revealed an initial decrease in signal, probably due to material equilibration after electrospinning, followed by a monotonic increase until it plateaued (Fig. 4B). An increase in Tyr fluorescence emission intensity can stem from a combination of several effects, such as less solvation of the residue, solvent polarity affecting protein conformation, medium viscosity restricting the movement of the residue, and low temperature. (Lakowicz, 2006). Tyr tends to preferentially bury in the protein interior via hydrophobic forces to reduce exposure to the hydrophilic solvent. Observed changes in the fluorescence intensity corresponded to protein structure reorganization correlated to the physical ageing of a polymer with a glass transition temperature above the storage temperature (Monnier et al., 2021). Polymer chain rearrangement effectively reduces the free volume in the matrix, facilitating the formation of inter/intra molecular bonds, which increases the brittleness of a material (Low et al., 2018). Although the Tyr fluorescence intensity signaled that protein rearrangements may be responsible for the increased rigidity and brittleness of the electrospun samples, the dependence of this measurement on probe concentration complicated its interpretation. Therefore, to verify the aforementioned trend, Tyr phosphorescence emission lifetimes were collected as this photophysical property is concentration-independent. Lifetimes exhibited a similar increase as intensity, with initial average lifetimes of 3.59 ± 0.14 and 5.38 ± 0.37 ms after 28 days, corresponding to a 50% increase compared to the recently produced material (Fig. 4A).

Besides monitoring Tyr emission, when excited at 270 nm, an additional band appeared at ~433 nm, which has been attributed to structural fluorescence arising from charge-transfer along a protein backbone with extensive β-sheet structures (del Mercato et al., 2007; Pinotsi et al., 2016). This emission band, tested under similar conditions, was also reported in zein/gluten doughs, particularly those with a high zein/gluten ratio due to the high β-sheets proportion in zein (Sadat et al., 2022). The emission intensity at 433 nm increased to a level similar to that of Tyr through time. This trend supports the hypothesis of protein rearrangements during storage.

Additionally, in the nonwovens, a decrease in the unordered random coil structures from 25 to 0% occurred within 10 days, while the ordered structures, particularly β-sheet, increased from 2 to 19% by the end of storage time as assessed with FTIR analysis (Fig. 5). These observations are in accordance with the results obtained using luminescence spectroscopy techniques. Less drastic effects observed over a shorter time were reported in a study on electrospun zein nonwovens that encapsulated epigallocatechin gallate, showing a notable increase in β-sheet structures with increasing storage times (Li et al., 2009). Ordered structures have been characterized as more rigid than unordered structures due to increased inter/intra protein bonds (Perticaroli et al., 2013; Skrbic et al., 2016). The increased proportion of β-sheet structure during storage aligns with previous reports on increased material rigidity and brittleness.

3.4. Chemical mapping of nonwovens

To better understand the changing protein-lipid distribution regarding a change in chemical bonds, Raman micro-spectroscopy was employed. Micrographs of the nonwovens immediately after manufacturing presented a relatively even distribution of protein (red)

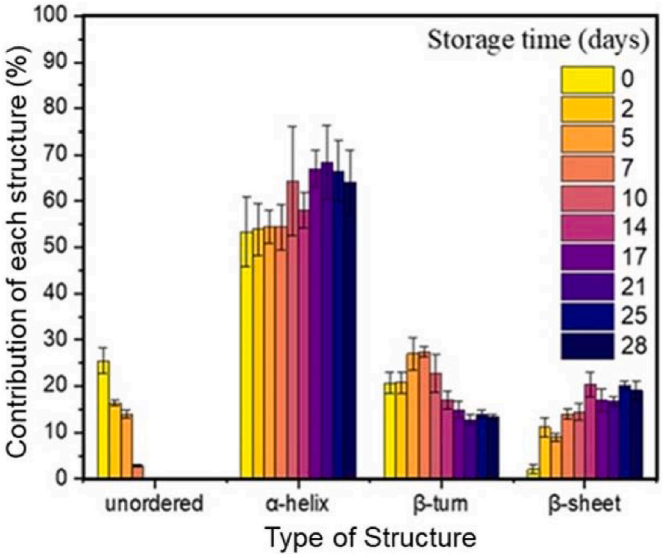

Fig. 5. Protein secondary structure distribution as a function of storage time, as calculated from the amide I region of the FTIR spectra.

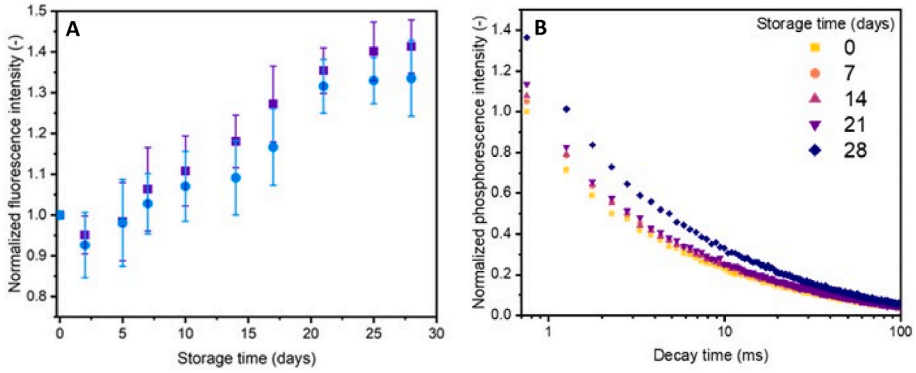

Fig. 4. A) Normalized fluorescence emission intensity of Tyr (λ_{exc} = 280 nm, purple squares) and 440 nm band (λ_{exc} = 350 nm, light blue circles) in zein nonwovens as a function of storage time. B) Tyr phosphorescence lifetimes in zein nonwovens during storage.

and lipid (blue) (Fig. 6A). Conversely, after 28 days of storage, distinct regions of higher lipid content appeared closer to the ribbon surface (Fig. 6B). After 28 days, the decrease in the intensity of the Raman band located at 3008 cm^{-1}, which corresponds to the unsaturated bonds in the vegetable oil, decreased by 47% suggesting lipid oxidation. The intensity ratio of the 1305 and 1267 cm^{-1} bands originated from the rocking of the -C-H bonds and the in-phase twisting of = C–H bonds, respectively and increased by 35%, indicating oxidation of the encapsulated corn oil (Muik et al., 2007).

Bands correlating to protein characteristics include the ratio of the peak intensities at 850 and 830 cm^{-1} and the intensity of the scatter band at 520 cm^{-1}, representing the Tyr doublet and disulfide bonds, respectively. In the electrospun fiber matrix, the ratio of the Tyr doublet signal decreased from 1.90 to 1.33, suggesting an increase in hydrogen bonding that correlated with a higher tensile strength in zein matrices (Turasan and Kokini, 2017). A 8% increase in the disulfide bond band was also observed, and while further investigation into the conformations of disulfide links is possible via deconvolution of the band at 520 cm^{-1}, due to the low signal-to-noise ratio obtained from extensive diffraction in the tested matrices, the deconvolution required excessive smoothing, potentially resulting in loss of signal (Wang et al., 2022). Therefore, the intensity at 520 cm^{-1} was directly used to benchmark the formation of disulfide bonds often formed due to the oxidation of cysteine amino acids, allowing inter/intra-molecular crosslinking (Joye et al., 2009). Oxidation can be speculated to be driven by secondary corn oil oxidation products or from the continual interaction of protein with molecular oxygen during storage. Chemical analysis of oxidative agents in the system throughout storage is needed to confirm this hypothesis.

3.5. Correlation and kinetics of the observed changes

A comparison of the measurements used to characterize physical (i.e., increased rigidity) and chemical (i.e., lipid oxidation) changes based on the fluorescence emission intensity of Tyr and BODIPY C11, respectively, contributes to elucidate the connection between these two phenomena. Plotting the normalized fluorescence intensity of Tyr vs. the oxidized BODIPY C11 revealed three phases that corresponded to the equilibration of the material with its environment, observable degradation, and finally, plateauing for both deteriorative phenomena (Fig. 7). This correlation highlights that rigidity and lipid oxidation changes follow a similar pattern and occur simultaneously. To better understand the timeline of the most relevant deteriorative effects in the nonwovens, the kinetics of the increase in matrix rigidity (i.e., the fluorescence intensity of the band at 430 nm), lipid oxidation (i.e., the fluorescence intensity of the oxidized BODIPY C11) and protein oxidation (i.e., the Raman band of the disulfide bonds), were characterized using Eq. (4). The experimental data adjusted with the logistic equation (Fig. 8), allow insights into the extent (Y_{max}), rate (k), and critical time (t_c) of each reaction (Corradini, 2018). Table 4 presents the parameters of Eq. (4) and the measures of goodness of fit.

As revealed in Fig. 7, lipid oxidation and increase in matrix rigidity exhibited similar kinetics and are well described by the selected

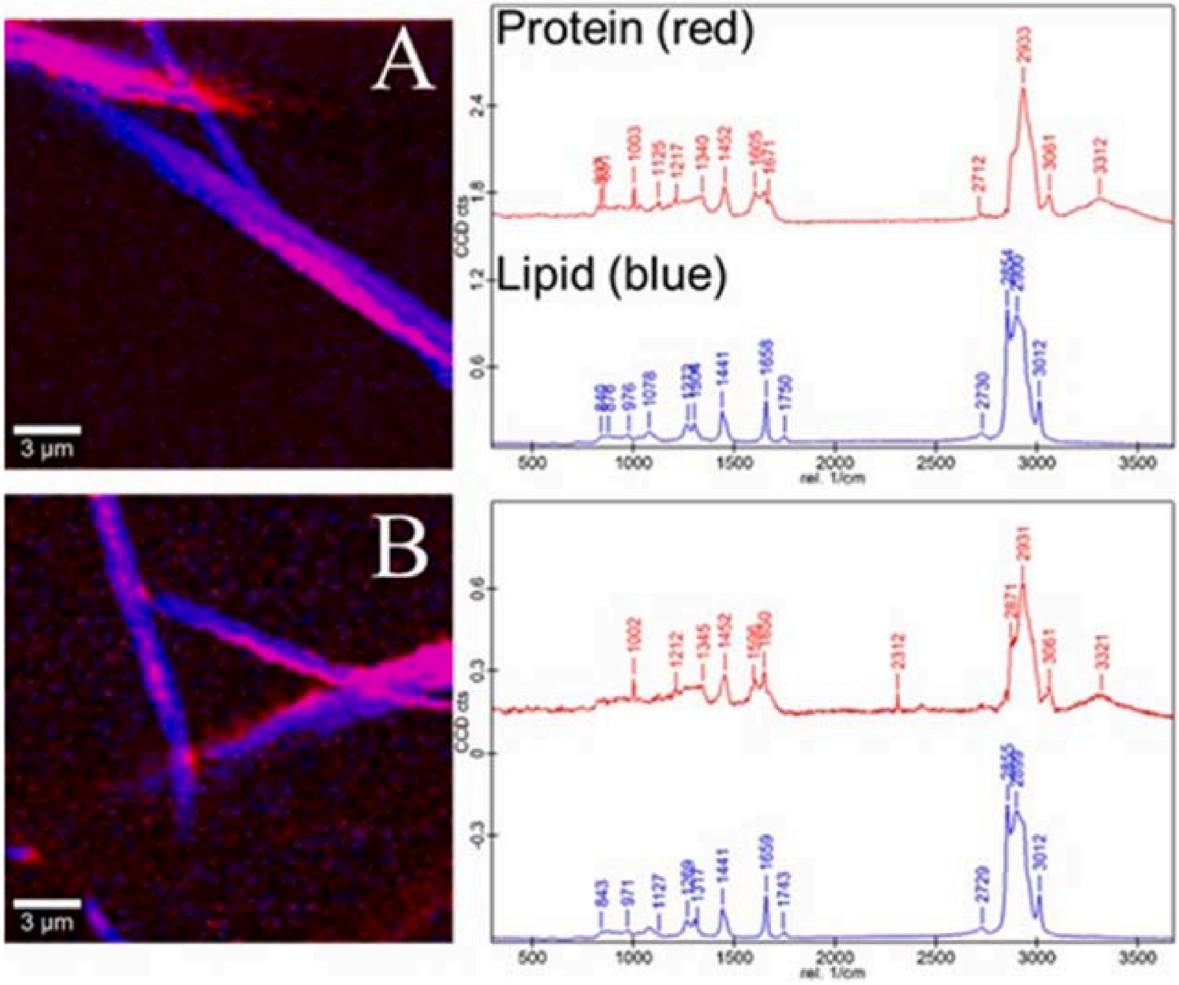

Fig. 6. Raman micrographs of electrospun zein with encapsulated corn oil after A) 0 and B) 28 days of storage. Red and blue spectra correspond to the protein and lipid, respectively.

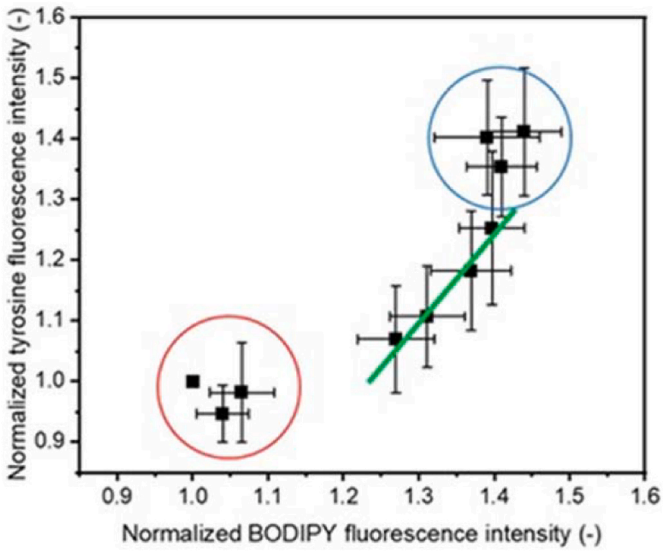

Fig. 7. Correlation between normalized fluorescence emission intensity of Tyr and BODIPY C11 in electrospun zein matrices during storage.

empirical model. Despite their similarity, scrutiny of the kinetic parameters revealed differences in the onset and rate of the respective phenomena, where an increase in rigidity preceded the onset of lipid oxidation, which, once initiated, accelerated. Conversely, disulfide bond formation proceeded slower than the other two phenomena, as evidenced by a rate an order of magnitude lower than the others.

From the data, it is inferred that electrospun zein nonwovens with encapsulated corn oil first underwent an equilibration stage that involved evaporation of the residual solvent from the zein matrix and redistribution in which the glassy protein polymer rearranges into more ordered secondary conformations with the formation of additional inter/intramolecular bonds. This rearrangement consequently displaced lipids from the core to the surface of the electrospun fibers, evidenced by the Raman mapping. Lipid oxidation proceeded at an increased rate due to the localized clusters of lipids near the surface of the fibers, wherein a thinner protein layer conferred less protection from oxygen. Protein rearrangement increased rigidity and brittleness as more disulfide bonds were formed, thereby resulting in fiber breakage. To conclude, the limiting stability of the corn-oil loaded electrospun zein nonwoven can be attributed to protein rearrangements that lead to changes in the distribution of oil across the ribbon structures, thereby altering the nonwovens mechanical properties, and modulating lipid/protein oxidation. Strategies to extend the stability of these materials should focus on slowing protein reorganization to deter the onset of physical ageing, which may decrease the rate of lipid oxidation and increase overall stability.

4. Conclusions

This research explored the efficacy of spectroscopic techniques to assess food quality attributes of novel materials, i.e., electrospun nonwovens, as a function of time. Investigating deterioration at multiple length scales uncovered the main phenomena and respective interrelated progression that limit their stability. SEM showed ribbon-like fibers where the diameter significantly decreased during storage (701 ± 23 nm vs. 620 ± 44 nm). Extensive fiber breakage correlated with increased brittleness, as reported from bulk and local measurements, e.g., decreased extensibility by 26%, increased Tyr emission intensity by 40% and phosphorescence lifetime by 50%. Changes in mechanical properties and matrix rigidity also correlated with a transition in zein secondary structures from unordered (25% vs. 0%) to ordered β-sheets (2% vs. 19%) during storage. Raman and luminescence micrographs

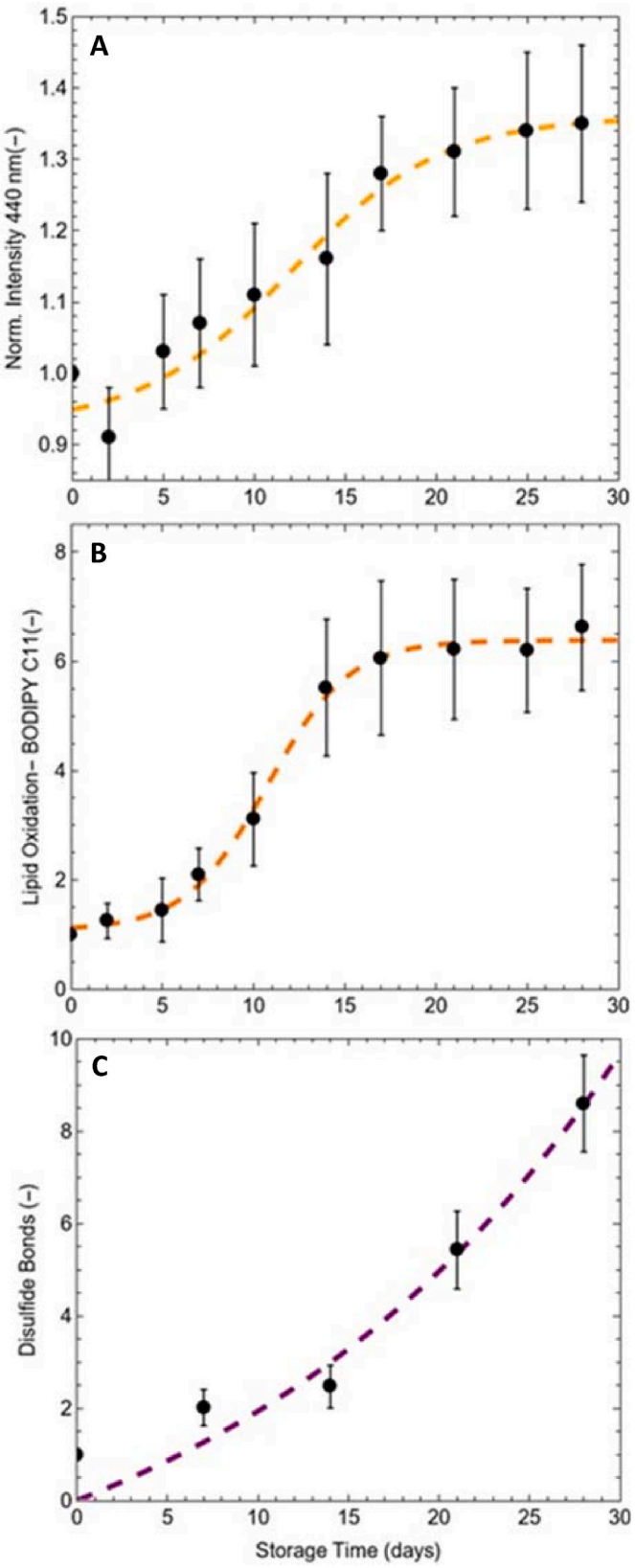

Fig. 8. A) Increased rigidity, represented by the intensity of the band at 440 nm, B) lipid oxidation, and C) disulfide bond formation as a function of storage time, fitted with Eq. 4. Filled circles: experimental data, dashed lines: adjusted fit.

Table 4
Kinetic parameters of the deteriorative processes in the nonwovens estimated using Eq. (4) as a model.

Attribute	Kinetic parameters (eq. (4))[a]			Goodness of fit (Adjusted R^2/MSE)
	Y_{max}	k ($days^{-1}$)	t_c (days)	
Molecular rigidity	1.35 (1.21, 1.56)	0.22 (0.02, 0.4)	11 (9.97, 11.55)	0.999/0.002
Lipid oxidation	6.42 (6.13, 6.72)	0.44 (0.31, 0.58)	12 (7.5, 16.5)	0.998/0.034
Disulfide bonds	15.6 (12.3, 18.9)	0.045 (0.001, 0.09)	127 (101, 153)	0.962/0.091

[a] 95 % confidence interval between brackets.

illustrate oil migration during storage, increasing lipid oxidation. The correlation between local rigidity and lipid distribution/oxidation suggests that protein structural reorganization increases material brittleness or propensity to physical breakage and displaces encapsulated oil into localized sites. Understanding the causes of deterioration aids in developing innovative strategies to improve the stability of these novel food-grade materials. It can also inform formulation and production to directly address deteriorative phenomena. The methods proposed herein to characterize deterioration at multiple length scales can track deteriorative mechanisms in other novel materials, expediting product development and extending product shelf-life.

CRediT authorship contribution statement

Louis A. Colaruotolo: Conceptualization, Methodology, Investigation, Formal analysis, Validation, Data curation, Writing – original draft, Visualization. **Singam Suranjoy Singh:** Methodology, Investigation. **Stacie Dobson:** Methodology, Investigation. **Loong-Tak Lim:** Conceptualization, Methodology, Resources, Writing – review & editing, Supervision. **Iris J. Joye:** Conceptualization, Resources, Writing – review & editing. **Michael A. Rogers:** Conceptualization, Resources, Visualization, Writing – review & editing. **Maria G. Corradini:** Conceptualization, Methodology, Formal analysis, Writing – original draft, Writing – review & editing, Visualization, Supervision, Project administration, Funding acquisition.

Declaration of competing interest

The authors declare the following financial interests/personal relationships which may be considered as potential competing interests:

Maria G. Corradini reports financial support was provided by NSERC. Maria G. Corradini reports a relationship with University of Guelph Arrell Food Institute that includes: employment. The corresponding author, Maria G. Corradini, is an associate editor for Current Research in Food Science Other authors declare that they have no known competing financial interests or personal relationships that could have appeared to influence the work reported in this paper.

Data availability

Data will be made available on request.

Acknowledgments

The authors acknowledge the financial support of the Natural Sciences and Engineering Research Council of Canada (NSERC) and the Canadian Innovation Fund (CFI). MGC and LAC would like to express gratitude to the Arrell Food Institute, the SMART Training Program and the Ontario Agricultural College at the University of Guelph for their support during this study.

References

Aceituno-Medina, M., Mendoza, S., Lagaron, J.M., Lopez-Rubio, A., 2013. Development and characterization of food-grade electrospun fibers from amaranth protein and pullulan blends. Food Res. Int. 54 (1), 667–674.

Aragao, G.M.F., Corradini, M.G., Peleg, M., 2008. A phenomenological model of the peroxide value's rise and fall during lipid oxidation. JAOCS (J. Am. Oil Chem. Soc.) 85, 1143. https://10.1007/s11746-008-1305-z.

Aytac, Z., Keskin, N.O.S., Tekinay, T., Uyar, T., 2017. Antioxidant alpha-tocopherol/gamma-cyclodextrin-inclusion complex encapsulated poly(lactic acid) electrospun nanofibrous web for food packaging. J. Appl. Polym. Sci. 134 (21), 9. https://doi.org/10.1002/app.44858, 44858.

Bajsic, E.G., Mijovic, B., Penava, N.V., Grguric, T.H., Slouf, M., Zdraveva, E., 2016. The effect of UV irradiation on the electrospun PCL/TiO_2 composites fibers. J. Appl. Polym. Sci. 133 (24), 9. https://doi.org/10.1002/app.43539, 43539.

Barrera-Arellano, D., Badan-Ribeiro, A.P., Serna-Saldivar, S.O., 2019. Corn oil: composition, processing, and utilization. In: Corn. AACC International Press, pp. 593–613. https://doi.org/10.1016/B978-0-12-811971-6.00021-8.

Calzada, J.F., Peleg, M., 1978. Mechanical interpretation of compressive stress-strain relationships of solid foods. J. Food Sci. 43 (4), 1087–1092. https://doi.org/10.1111/j.1365-2621.1978.tb15240.x.

Cavaliere, A., Ventura, V., 2018. Mismatch between food sustainability and consumer acceptance toward innovation technologies among Millennial students: the case of shelf life extension. J. Clean. Prod. 175, 641–650. https://doi.org/10.1016/j.jclepro.2017.12.087.

Colaruotolo, L., 2019. Optical Meets Mechanical: Use of Luminescence Spectroscopy to Assess Ageing in Biodegradable Films. University of Massachusetts, Amherst. https://doi.org/10.7275/15118552.

Colaruotolo, L.A., Peters, E., Corradini, M.G., 2021. Novel luminescent techniques in aid of food quality, product development, and food processing. Curr. Opin. Food Sci. 42, 148–156. https://doi.org/10.1016/j.cofs.2021.06.005.

Corradini, M.G., 2018. Shelf life of food products: from open labeling to real-time measurements. Annu. Rev. Food Sci. Technol. 9, 251–269. https://doi.org/10.1146/annurev-food-030117-012433.

Corradini, M.G., Peleg, M., 2006. Direction reversals in the mechanical signature of cellular snacks: a measure of brittleness? J. Texture Stud. 37 (5), 538–552. https://doi.org/10.1111/j.1745-4603.2006.00067.x.

Corradini, M.G., Demol, M., Boeve, J., Ludescher, R.D., Joye, I.J., 2017. Fluorescence spectroscopy as a tool to unravel the dynamics of protein nanoparticle formation by liquid antisolvent precipitation. Food Biophys. 12 (2), 211–221. https://doi.org/10.1007/s11483-017-9477-4.

del Mercato, L.L., Pompa, P.P., Maruccio, G., Rinaldi, R., 2007. Charge transport and intrinsic fluorescence in amyloid-like fibrils. Proc. Natl. Acad. Sci. USA 104 (46), 18019–18024. https://doi.org/10.1073/pnas.0702843104.

Domínguez-Rebolledo, Á., Martínez-Pastor, F., Fernández-Santos, M.R., Del Olmo, E., Bisbal, A., Ros-Santaella, J.L., Garde, J.J., 2010. Comparison of the TBARS assay and BODIPY C11 probes for assessing lipid peroxidation in Red Deer spermatozoa. Reprod. Domest. Anim. 45 (6), e360–e368. https://doi.org/10.1111/j.1439-0531.2009.01578.x.

Draganski, A.R., Corradini, M.G., Ludescher, R.D., 2015. Revisiting time-resolved protein phosphorescence. Appl. Spectrosc. 69 (9), 1074–1081. https://doi.org/10.1366/14-07799.

Drosou, C., Krokida, M., Biliaderis, C.G., 2022. Encapsulation of β-carotene into food-grade nanofibers via coaxial electrospinning of hydrocolloids: enhancement of oxidative stability and photoprotection. Food Hydrocolloids 133, 107949. https://doi.org/10.1016/j.foodhyd.2022.107949.

Fantini, G.A., Yoshioka, T., 1992. Use and limitations of thiobarbituric acid reaction to detect lipid peroxidation. Am. J. Physiol.-Heart C 263 (3), H981–H983. https://doi.org/10.1152/ajpheart.1992.263.3.H981.

García Moreno, P.J., Boutrup Stephansen, K., van derKruijs, J., Guadix, A., Guadix, E.M., Chronakis, I.S., Jacobsen, C., 2016. Encapsulation of fish oil in nanofibers by emulsion electrospinning: physical characterization and oxidative stability. J. Food Eng. 183, 39–49. https://doi.org/10.1016/j.jfoodeng.2016.03.015.

Grant, K.R., Gallardo, R.K., McCluskey, J.J., 2021. Consumer preferences for foods with clean labels and new food technologies. Agribus 37 (4), 764–781. https://doi.org/10.1002/agr.21705.

Hadad, S., Goli, S.A.H., 2019. Improving oxidative stability of flaxseed oil by encapsulation in electrospun flaxseed mucilage nanofiber. Food Bioprocess Technol. 12, 829–838. https://doi.org/10.1007/s11947-019-02259-1.

Joye, I.J., Lagrain, B., Delcour, J.A., 2009. Endogenous redox agents and enzymes that affect protein network formation during breadmaking - a review. J. Cereal. Sci. 50 (1), 1–10. https://doi.org/10.1016/j.jcs.2009.04.002.

Lakowicz, J.R., 2006. Introduction to Fluorescence Spectroscopy, third ed. Springer. https://doi.org/10.1007/978-0-387-46312-4_1.

Laurindo, J.B., Peleg, M., 2008. Mechanical characterization of shredded wheat. J. Texture Stud. 39 (5), 444–459. https://doi.org/10.1111/j.1745-4603.2008.00153.x.

Li, Y., Lim, L.T., Kakuda, Y., 2009. Electrospun zein fibers as carriers to stabilize (-)-epigallocatechin gallate. J. Food Sci. 74 (3), C233–C240. https://doi.org/10.1111/j.1750-3841.2009.01093.x.

Lim, L.-T., Mendes, A.C., Chronakis, I.S., 2019. Electrospinning and electrospraying technologies for food applications. Adv. Food Nutr. Res. 88, 167–234. https://doi.org/10.1016/bs.afnr.2019.02.005.

Liu, Q., Huang, H., Chen, H., Lin, J., Wang, Q., 2019. Food-grade nanoemulsions: preparation, stability, and application in encapsulation of bioactive compounds. Molecules 24 (23), 4242. https://doi.org/10.3390/molecules24234242.

Low, Z.-X., Budd, P.M., McKeown, N.B., Patterson, D.A., 2018. Gas permeation properties, physical aging, and its mitigation in high free volume glassy polymers. Chem. Rev. 118 (12), 5871–5911. https://doi.org/10.1021/acs.chemrev.7b00629.

Menaka, T., Srinivasan, A., 2023. Electrospinning with curved nozzle spinneret for producing poly (vinyl Alcohol) nanomembrane for filtration. Mater. Res. Express 10, 045305. https://doi.org/10.1088/2053-1591/acc788.

Merrick, M.M., Sujanani, R., Freeman, B.D., 2020. Glassy polymers: historical findings, membrane applications, and unresolved questions regarding physical aging. Polym. 211 (C), 123176 https://doi.org/10.1016/j.polymer.2020.123176.

Monnier, X., Marina, S., Lopez de Pariza, X., Sardón, H., Martin, J., Cangialosi, D., 2021. Physical aging behavior of a glassy polyether. Polym 13 (6), 954. https://doi.org/10.3390/polym13060954.

Moomand, K., Lim, L.T., 2014. Oxidative stability of encapsulated fish oil in electrospun zein fibres. Food Res. Int. 62, 523–532. https://doi.org/10.1016/j.foodres.2014.03.054.

Moomand, K., Lim, L.T., 2015. Effects of solvent and n-3 rich fish oil on physicochemical properties of electrospun zein fibres. Food Hydrocolloids 46, 191–200. https://doi.org/10.1016/j.foodhyd.2014.12.014.

Muik, B., Lendl, B., Molina-Diaz, A., Valcarcel, M., Ayora-Cañada, M.J., 2007. Two-dimensional correlation spectroscopy and multivariate curve resolution for the study of lipid oxidation in edible oils monitored by FTIR and FT-Raman spectroscopy. Anal. Chim. Acta 593 (1), 54–67. https://doi.org/10.1016/j.aca.2007.04.050.

Pedram Rad, Z., Mokhtari, J., Abbasi, M., 2018. Fabrication and characterization of PCL/zein/gum Arabic electrospun nanocomposite scaffold for skin tissue engineering. Mater. Sci. Eng. C 93, 356–366. https://doi.org/10.1016/j.msec.2018.08.010.

Perticaroli, S., Nickels, J.D., Ehlers, G., O'Neill, H., Zhang, Q., Sokolov, A.P., 2013. Secondary structure and rigidity in model proteins. Soft Matter 28 (40), 9548–9556. https://doi.org/10.1039/c3sm50807b.

Pinotsi, D., Grisanti, L., Mahou, P., Gebauer, R., Kaminski, C.F., Hassanali, A., Kaminski Schierle, G.S., 2016. Proton transfer and structure-specific fluorescence in hydrogen bond-rich protein structures. JACS 138 (9), 3046–3057. https://doi.org/10.1021/jacs.5b11012.

Plackett, D.V., 2011. Biopolymers New Materials for Sustainable Films and Coatings, first ed. Wiley.

Prahasti, G., Zulfi, A., Munir, M.M., 2020. Needleless electrospinning system with wire spinneret: an alternative way to control morphology, size, and productivity of nanofibers. Nano Ex 1, 010046. https://doi.org/10.1088/2632-959X/ab976a.

Seethu, B., Pushpadass, H.A., Emerald, F.M.E., Nath, B.S., Naik, N.L., Subramanian, K., 2020. Electrohydrodynamic encapsulation of resveratrol using food-grade nanofibres: process optimization, characterization, and fortification. Food Bioprocess Technol. 13 (2), 341–354. https://doi.org/10.1007/s11947-019-02399-4.

Shah, Y.A., Bhatia, S., Al-Harrasi, A., Afzaal, M., Saeed, F., Anwer, M.K., Khan, M.R., Jawad, M., Akram, N., Faisal, Z., 2023. Mechanical properties of protein-based food packaging materials. Polym 15 (7), 1724. https://doi.org/10.3390/polym15071724.

Skrbic, T., Hoang, T.X., Giacometti, A., 2016. Effective stiffness and formation of secondary structures in a protein-like model. J. Chem. Phys. 145 (8), 084904 https://doi.org/10.1063/1.4961387.

Steffe, J.F., 1996. Rheological Methods in Food Process Engineering, second ed. Freeman Press.

Struik, L.C.E., 1977. Physical Aging in Amorphous Polymers and Other Materials. Elsevier Science Ltd.

Taherimehr, M., YousefniaPasha, H., Tabatabaeekoloor, R., Pesaranhajiabbas, E., 2021. Trends and challenges of biopolymer-based nanocomposites in food packaging. Compr. Rev. Food Sci. Food Saf. 20 (6), 5321–5344. https://doi.org/10.1111/1541-4337.12832.

Tang, Y.D., Zhou, Y., Lan, X.Z., Huang, D.C., Luo, T.T., Ji, J.J., Mafang, Z., Miao, X., Wang, H., Wang, W., 2019. Electrospun gelatin nanofibers encapsulated with peppermint and chamomile essential oils as potential edible packaging. J. Agric. Food Chem. 67 (8), 2227–2234. https://doi.org/10.1021/acs.jafc.8b06226.

Turasan, H., Kokini, J.L., 2017. Advances in understanding the molecular structures and functionalities of biodegradable zein-based materials using spectroscopic techniques: a review. Biomacromolecules 18 (2), 331–354. https://doi.org/10.1021/acs.biomac.6b01455.

Ullsten, N.H., Gällstedt, M., Hedenqvist, M.S., 2016. Plasticizers for protein-based materials. In: El-Amin, M. (Ed.), Viscoelastic and Viscoplastic Materials. IntechOpen, London, UK, pp. 81–101.

Wang, Y.H., Zhao, M., Barker, S.A., Belton, P.S., Craig, D.Q.M., 2019. A spectroscopic and thermal investigation into the relationship between composition, secondary structure, and physical characteristics of electrospun zein nanofibers. Mater. Sci. Eng. C 98, 409–418. https://doi.org/10.1016/j.msec.2018.12.134.

Wang, Q., Tang, Y., Yang, Y., Lei, L., Lei, X., Zhao, J., Zhang, Y., Li, L., Wang, Q., Ming, J., 2022. Interactions and structural properties of zein/ferulic acid: the effect of calcium chloride. Food Chem. 373 (Part B) https://doi.org/10.1016/j.foodchem.2021.131489, 131489-131489.

Xu, W., Karst, D., Yang, W., Yang, Y., 2008. Novel zein-based electrospun fibers with the water stability and strength necessary for various applications. Polym. Int. 57, 1110–1117. https://doi.org/10.1002/pi.2450.